

# GPE – A COMPACT GAMMA-RAY POLARIMETER WITH ENERGY RECONSTRUCTION CAPABILITY

A. S. CUCOANES<sup>1</sup>, M. CUCIUC<sup>1</sup>, Y. ARAI<sup>2</sup>, K. HOMMA<sup>3</sup>, Y. NAKAMIYA<sup>1</sup>, O. TESILEANU<sup>1,\*</sup>

<sup>1</sup> Extreme Light Infrastructure – Nuclear Physics (ELI-NP), Horia Hulubei National Institute for Physics and Nuclear Engineering, 30 Reactorului street, RO-077125 Magurele, Romania

*E-mails:* andi.cucoanes@eli-np.ro, mihai.cuciuc@eli-np.ro,  
yoshihide.nakamiya@eli-np.ro, ovidiu.tesileanu@eli-np.ro

<sup>2</sup> Institute of Particle and Nuclear Studies, High Energy Accelerator Research Organization (KEK), 1-1 Oho, Tsukuba 305-0801, Japan

*E-mail:* yasuo.arai@kek.jp

<sup>3</sup> Graduate School of Advanced Science and Engineering, Hiroshima University, Kagamiyama, Higashi-Hiroshima, 739-8526, Japan

*E-mail:* khomma@hiroshima-u.ac.jp

\* *Corresponding author, E-mail:* ovidiu.tesileanu@eli-np.ro

*Received December 14, 2023*

*Abstract.* We present here the design, expected parameters and performance tests of a compact detector, based on INTPIX4 sensing device, developed in the framework of the Extreme Light Infrastructure – Nuclear Physics (ELI-NP) project, capable of measuring both polarization and energy of gamma rays, in the high energy range above 1 GeV. The detector, based on electron-positron pair creation in the Bethe-Heitler process, has been tested with cosmogenic muons and will allow unique experiments at the ELI-NP facility.

*Key words:* gamma rays, polarization, pair creation.

DOI: <https://doi.org/10.59277/RomJPhys.2024.69.401>

## 1. INTRODUCTION

Several future experiments based on high power and short pulse lasers involve the generation of high energy polarized photons, bringing a new focus on the challenging topic of high energy gamma polarimetry. In the near future, the ELI-NP [1] facility in Romania will provide unique investigations of intensity regimes up to  $\sim 10^{23}$  W/cm<sup>2</sup>, with the help of two 10 PW laser beams. Albeit several orders of magnitude below the Schwinger limit ( $\sim 10^{29}$  W/cm<sup>2</sup>) [2], this intensity regime opens the way for the experimental study of theoretically anticipated QED phenomena, such as radiation reaction and assisted pair production, at the collision between the high intensity laser pulse and high energy electrons (created *via* laser wakefield acceleration LWFA [3]). In these experiments, a high interest is the measurement of polarization and energy of the resulting photons, at near-GeV or GeV scale.

At such high gamma energies, the most significant interaction mechanism is the conversion into an electron-positron pair, in the presence of a nuclear field

(nuclear pair conversion) or an electronic field (triplet conversion), the former dominating over the latter. As first shown in the '50s [4, 5], the kinematics of this reaction can resolve the polarization of the incoming photon. In the case of nuclear pair conversion and for high  $Z$  materials, the nuclear recoil is small and the trajectories are nearly coplanar [6]. The azimuthal angle of this plane depends on the polarization direction of the incoming photon, thus an asymmetry in its distribution provides a measure of the linear gamma polarization. The angular deflection of the  $e^+e^-$  emission plane is described by [7, 8]:

$$dN_{e^+e^-}^{pol}/d\omega = N_{e^+e^-}^{unpol} [1 + P_l A \cos(2(\omega - \omega_0))] \quad (1)$$

where  $N_{e^+e^-}^{unpol}$  is the number of pairs in the unpolarized case,  $\omega$  is the azimuthal scattering angle and  $\omega_0$  is the angle of the polarization plane with respect to the reference plane, in the laboratory frame. We also consider  $\omega_0 = 0$ , since the polarization plane of the gamma-rays is strongly correlated to that of the laser and the reference plane of the detection system should match it (see for example [9] for a discussion when  $\omega_0$  is unknown). The modulation factor,  $P_l A$ , is the product between the degree of linear polarization  $P_l$  and the analyzing power  $A$ , a parameter given by the degradation of the measured asymmetry, as a consequence of the finite experimental resolution. Both,  $A$  and  $P_l$  can take values between 0 and 1. The azimuthal angle is defined between the gamma polarization plane and the pair emission plane. Ideally, the intersection of these planes contains the interaction point (Fig.1–left), however, since reaction products could suffer scatterings in the material after interaction, their trajectories could be affected, as shown in Fig.1–right.

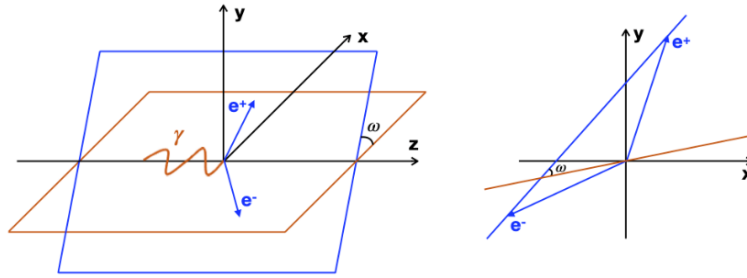


Fig. 1 – The azimuthal scattering angle is defined (left figure) as the angle between the plane of gamma ray polarization (orange) and the plane of electron-positron pair creation (blue). Since the pair particles could suffer scatterings inside the material, the plane distribution on the beam direction is modified, as shown in the figure on the right.

Equation (1) is used to fit the angular distribution of the  $e^+e^-$  pairs, *i.e.* the azimuthal angle distribution, in this case the product  $P_l A$  being a free parameter.

Polarimetry is often used in astrophysical investigations, providing information on the magnetic fields, in the region where energetic gamma rays are emitted.

Consequently, several gamma polarimeters, mainly based on Compton scattering or photoelectric absorption, have been used up to now [9] in this research direction. In the pair production regime, a notable example is HARPO [10], a TPC-based detector able to provide polarization measurements of photons below 50 MeV. At JLab, a detector based on micro-strip detectors and drift chambers capable of reconstructing  $e^+e^-$  events for determining GeV gamma polarization was proposed in [11] and was tested at SPring-8/LEPS.

Such measurements face important challenges. Let us consider a Converter layer where the conversion of gamma to electron-positron pair occurs (see Section 2), and several detector layers where the positions of the electron and positron are recorded for track reconstruction. The reaction products,  $e^+$  and  $e^-$ , undergo significant multiple scatterings in each detector layer, affecting the polarization measurement. At low fluxes of the incoming gamma radiation, the small thickness of the Converter layer where the pair production is assumed to happen, is disfavored by the small cross-section, while an increased thickness favors multiple scatterings. At high fluxes, the thickness of the converter layer has to be much reduced, in order to avoid pile-up events which would make track reconstruction difficult because of the increased number of hit combinations. However, in the high-flux regime the pair creation may occur in the detection layers themselves, reducing the ratio of the successfully reconstructed events in the total.

These two flux regimes are characteristic for the main applications of a compact polarimeter: the measurement at low flux of high energy gamma photons of astrophysical origin and, respectively, the polarization measurement under incidence of multiple gamma rays generated in laser interactions. Although our development of the GPE aims to tackle the challenges of the laser-based experiments, the compact design and low mass of the proposed detector represent features which could become important if this type of detector will be developed for various other experimental systems such as space missions.

In the next sections we will outline the design and the main performance figures of GPE, a detector capable of measuring both the polarization and the energy of GeV gamma-rays. Indeed, by reconstructing the reaction kinematics from the particle tracks, the energy of the incoming photon can be deduced, simultaneously to polarization.

## 2. THE GPE DESIGN AND VALIDATION

With an overall dimension of  $80 \times 30 \times 30$  cm<sup>3</sup>, GPE is compact and movable, allowing a high degree of flexibility for various experimental setups.

The detector itself can be viewed as a fixed target experiment, where the incoming gamma beam (GB) produces the electron-positron pairs in a first layer called Converter. When measuring low to moderate flux of high-energy gamma

photons in a laser-based experiment, this first layer can be itself a detector – in the case of the GPE, a first Silicon pixelated detector layer (Fig. 2). The pair-creation probability is  $\sim 2 \times 10^{-3}$  above 1 GeV photon energy for the Converter layer thickness of 250 microns. The Converter is composed of pixel arrays with pixel dimensions of  $17 \times 17 \mu\text{m}^2$  and, as shown later, it accomplishes two roles, as converter material for the pair creation and also as vertex detector. Vertex determination is embedded in the track reconstruction for the removal of unexpected off-vertex events, or of events originating in different detector layers. The Converter thickness, given in our case by the availability of the sensors, is a critical parameter of the detector, influencing the number of produced pair events, but also to the analyzing power due to the straggling of the pair products.

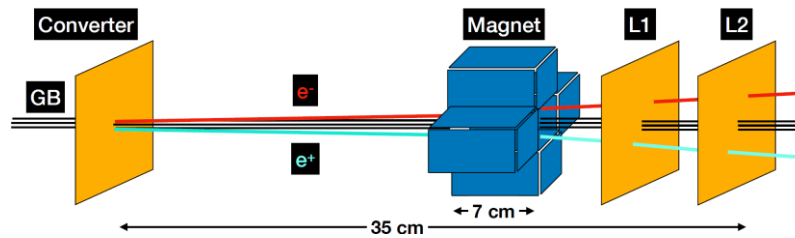


Fig. 2 – GPE detector schematic.

The electron and positron created at the Converter are further separated by a 0.8 T magnetic field and reach a second sensitive part of the assembly, comprising two pixelated layers L1 and L2, placed parallel to the Converter. The parameters of the incoming photon are obtained from track reconstruction of both the electron and the positron, using the information given by all detector layers: the active Converter provides the interaction vertex, and the L1–L2 layers give the positions of the  $e^+e^-$  hits at two downstream locations. Taking into consideration the above-mentioned pair creation probability, it follows that the GPE can be used with good results in gamma photon fluxes up to about  $10^3$  photons / pulse. Beyond this value, due to high combinatorial background (*i.e.* fake track reconstruction), an additional layer is needed to verify the reconstruction based on the first two layers.

The detector chassis is built from an extruded aluminum profile that creates a configurable frame, allowing the repositioning of the sensors and the magnet for energy range adjustment.

The performance of the detector hinges mainly on the strength and uniformity of the magnetic field as well as on the pixel size and the thickness of its layers. The strength of the magnetic field is the result of a compromise between the detector resolution and the acceptance for low energy pairs. For a compact magnet system with excellent uniformity and high strength, a Halbach array configuration built with Neodymium-based permanent magnets of  $25 \times 25 \times 70 \text{ mm}^3$  is implemented. Shown in Fig. 3, this configuration provides a uniform transverse field of 0.8 T in the central

region, the field configuration being simulated in COMSOL<sup>®</sup> and then imported in our Geant4 simulations. The magnet is the dominant element of the detector weight, giving unavoidable constraints for the total weight of the system.

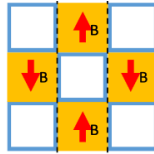


Fig. 3 – Transversal section of the magnet configuration: the yellow squares represent individual Neodymium bars and the blue lines show the (aluminum) frame of the magnet. The lateral dimension is 2.5 cm, for all square sections in the figure: Al frames and magnet bars. The total length of the configuration (along the axis perpendicular on this drawing) is 7 cm.

For the detection layers, following a search of what was currently available and with further development perspectives, we have chosen the pixelated INTPIX4 chips [13, 14], developed at KEK, Japan, having a resolution of  $832 \times 512$  pixels and a thickness of  $250 \mu\text{m}$ . This standard thickness can be reduced after the production of the chips by applying a thinning process to the wafer, which was tested at KEK with good results down to below  $100 \mu\text{m}$ . Future upgrades of the GPE, aiming for the accommodation of larger gamma photon flux, will feature these thinned chips, for the reasons discussed above.

Each pixel is  $17 \times 17 \mu\text{m}^2$  and the chip includes pixel charge storage and addressing circuitry to allow exposure control as well as routing to analog outputs. Readout of the chips is handled by SEABAS2 [14–16] boards, which provide high-throughput links to a DAQ computer, as well as an open FPGA that accommodates the user logic for multi-board synchronization or external signaling. Hardware handshaking between the three SEABAS2 boards was implemented in order to keep events synchronized, as nondeterministic software latencies in the DAQ computer could cause event misalignment. The overall data flow is summarized in Fig. 4.

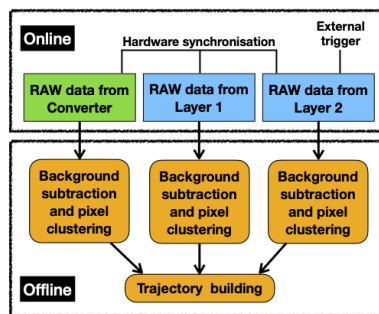


Fig. 4 – The data flow schematic. Each silicon sensor produces its own ROOT [18] data file and background subtraction and pixel clustering is running on them, individually. Subsequently, they are merged into a single data stream for trajectory building.

Sensor RAW data are delivered by each INTPIX4 chip [17] for each trigger: one data frame and 49 subsequent pedestal frames. The data for each chip is then processed offline to perform background subtraction and pixel clustering. The obtained detector hits are used to reconstruct charged particle trajectories.

In order to test the detector electronics, DAQ and the reconstruction algorithm, the measurement of cosmogenic muons was performed. In this setup, shown in Fig. 5, the detector was triggered by fast detectors: avalanche tubes and scintillators, arranged in a geometry that allows the coincidence with the INTPIX4 sensors. The coincidence signal of the avalanche tubes and scintillators is fed into the master readout FPGA and, if this signal falls within the integration window, it triggers the readout of all 3 boards. In a laser-based experiment setup the trigger shall be given by the laser system, to synchronize detection with the laser pulse.

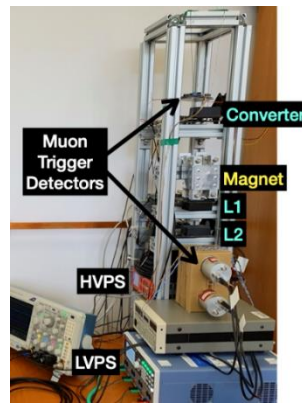


Fig. 5 – Setup for the cosmic muon measurement. GPE (Converter+Magnet+L1+L2) is placed between the detectors which create the muon trigger: one Geiger-Muller detector on the upper side and two LaBr(Ce) detectors on the lower side. The High Voltage power supply (HVPS) is connected to muon trigger detectors and the Low Voltage power supply to the GPE acquisition boards.

Once the data corresponding to each valid trigger is saved on disk, the acquisition pipeline shown in Fig. 4 starts the background subtraction and pixel clustering, applied independently to each sensor, in order to produce a set of cluster hits for each event. The events containing at least one hit in each sensor are selected for reconstruction.

During the first part of the data-taking, the alignment of the detector sensors is carried out by using straight line trajectories of muons, in all 3 projections, hence the magnet is not used. The detector dead-time is given mainly by the duration of the reset state which clears the charge collected by the sensors, and has a value of 66% from the real time, as computed from the sensor integration time.

During the second part, adding the magnetic field, the muon trajectories are bent and the particle energy and charge can be inferred from the track geometry using a reconstruction code written in ROOT.

### 3. SIMULATION AND RECONSTRUCTION; EXPECTED PARAMETERS FOR HIGH ENERGY GAMMAS

As previously described, the data provided by the DAQ system represents particle trajectories in the detector. Further on, the reconstruction algorithm verifies the track combinations, identifying the ones that correspond to the characteristics of a Bethe-Heitler process produced in the Converter. As the format is identical for experimental and simulated data, the reconstruction code can process them in the same way, facilitating the comparison and validation.

The detector performance figures for high-energy gamma rays are computed by implementing the detector design (Fig. 2) in a Geant4 v.10.02 [19–21] code, where the *G4BetheHeitlerModel* class was modified to include the description of the photon polarization. We scanned 12 monoenergetic points from 1 to 10 GeV and 5 polarization values, for gamma events generated orthogonally on the Converter surface, in a spot size of 3 mm. Each of the 60 simulated runs contains  $10^7$  events.

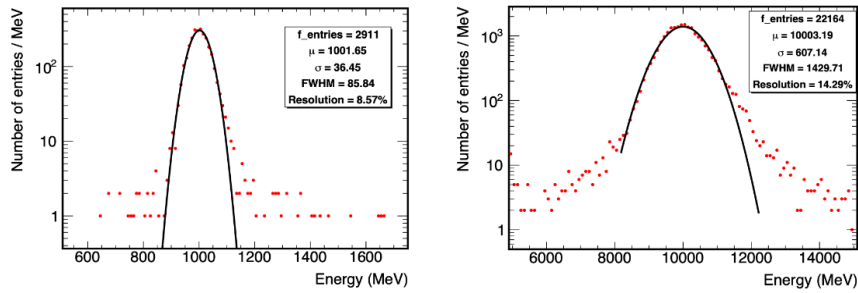


Fig. 6 – Reconstructed energy for monoenergetic gamma rays: left:  $E_\gamma = 1$  GeV and right:  $E_\gamma = 10$  GeV. In each case,  $10^7$  gamma events were simulated from which a part ( $f\_entries$ ) was reconstructed, according to Eq. (2). The parameters of Gaussian fits are shown in the legend,  $\mu = E_{reco}$  [MeV].

The quality of energy reconstruction for gammas of 1 and 10 GeV is shown in Fig. 6, where the red points show the reconstructed values and the black lines are Gaussian fits for the distributions. Figure 6 shows both the increase in the number of reconstructed events and the distribution widening at higher energies, asymmetrically with larger wings towards the high-energy side, as expected due to the decreasing deviation angles. Nonetheless, the residual values  $(E_{reco} - E_\gamma)/E_\gamma$ , corresponding to the whole energy range, are less than 0.4%.

The total number of reconstructed events increases with the energy as shown in Fig. 7–left and is essentially varying as:

$$N_{pair} \sim \sigma_{pair} \epsilon_{pair} \epsilon_{reco} \quad (2)$$

where  $\sigma_{pair}$  is the cross-section of the Bethe-Heitler process,  $\epsilon_{pair}$  is the detection efficiency of  $e^+e^-$  pairs, and  $\epsilon_{reco}$  is the reconstruction efficiency. At low energy,

the main influence is given by the detection efficiency, since the curvature of the lepton trajectories induced by the magnet combined with the limited dimensions of the sensors could result in loss of events. At high energy, the fraction of reconstructed events is approaching the value given by the cross-section, with the downside of energy resolution degradation (Fig. 7–right), due to the decrease in the curvature of the particle trajectories (as a consequence of the limited bending power of the magnet) combined with the finite pixel granularity of L1 and L2 layers.

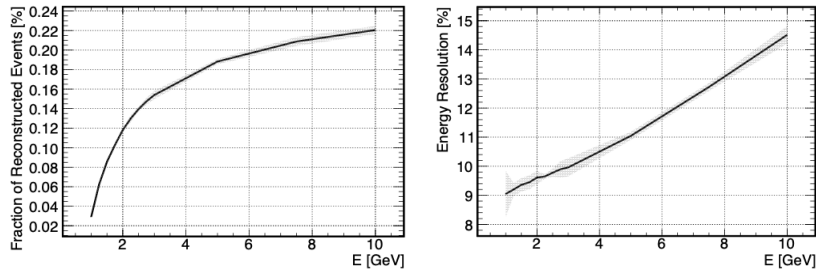


Fig. 7 – GPE detector parameters obtained from the reconstruction of simulated gamma events: left- the fraction of reconstructed to generated events and right- energy resolution. For each simulated energy (12 values), 5 runs of  $10^7$  events were generated. For each energy, the black line links the mean values, and the shadow regions show the difference between the minimum and the maximum values.

Gamma events with various energies and polarizations produce specific azimuthal angle distributions following Eq. (1) and the energy dependence of the pair production cross section. This angle is computed using:

$$\omega = \text{Arctan} \left( \frac{p_{e^+}^y - p_{e^-}^y}{p_{e^+}^x - p_{e^-}^x} \right) \quad (3)$$

where the transversal components of the  $e^+$  and  $e^-$  momenta are reconstructed from the hits in detector layers;  $x$  and  $y$  directions are perpendicular, respectively parallel to the magnetic field direction.

Figure 8 shows the superpositions of the azimuthal angle distributions, on one hand from the parameters of the particles generated in the Bethe-Heitler process provided directly by Geant4 (“*Truth*”) and on the other hand after the momenta reconstruction (“*Reco*”) of the pair particles. The “*Reco*” distributions for non-zero polarization are fitted with equation:

$$dN_{e^+e^-}^{pol} / d\omega = N_{e^+e^-}^{unpol} [1 + (P_l A + B) \cos(2(\omega - \omega_0))] \quad (4)$$

where the  $B$  is an offset term obtained from Eq. (4) at null polarization ( $P_l = 0$ ), in order to account for the residual value due to the asymmetry of the track reconstruction in the transversal plane of the beam direction. This reconstruction is

influenced by the asymmetry of the magnetic field in the  $x$  versus  $y$  directions of the transversal plane. The “Reco” distribution has two free parameters:  $N_{e^+e^-}^{unpol}$  and  $P_l A$  and then it is renormalized to  $N_{e^+e^-}^{unpol}$  for a better comparison. As the energy of the gamma events increases, the number of reconstructed events also increases (following the dependence shown in Fig. 7–left) and, in consequence, the magnitude of the “Reco” error bars decreases.

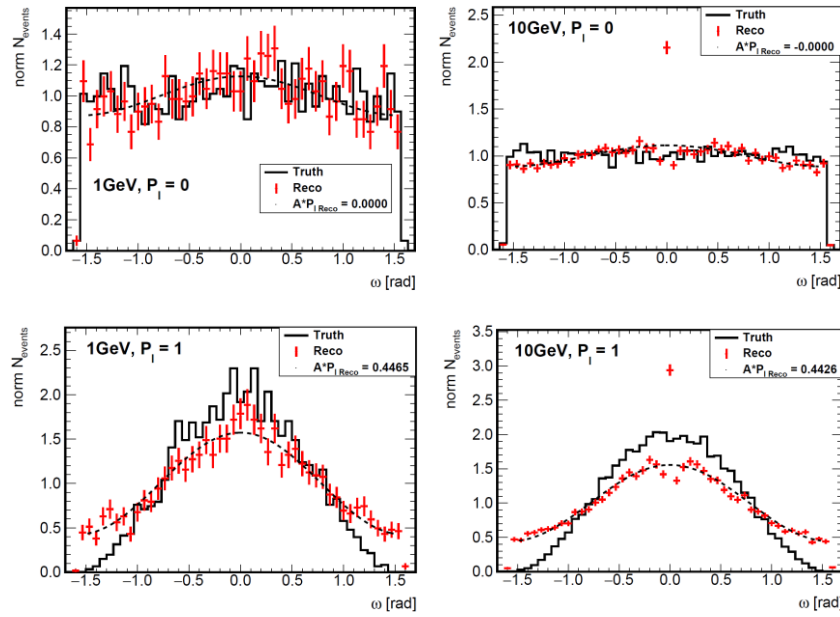


Fig. 8 – Fits to azimuthal distributions of simulated gamma events. “Truth” and “Reco” represent the distributions directly computed from the Geant4 momentum parameters and respectively reconstructed from the detector hits. The fit with Eq. 4 on “Reco” distribution delivers the shown  $P_l A$  values.

For comparison, “Truth” contains a selection of events which were reconstructed.

The pair creation at high energy tends to be boosted in the forward direction, resulting in low transverse momenta of the produced particles. In addition, at high energy, the multiple scatterings are less likely, resulting also in transverse momenta reduction. Moreover, the influence of the magnetic field on  $x$ -direction results in a high probability that hits in the L1 layer to be placed on the same horizontal row of pixels (constant  $y$ ). Such events are reconstructed with a null  $\omega$  value (see Fig. 8, 10 GeV plots) and consequently, the artifact at  $\omega = 0$  is formed for the higher energies because of the layers granularity on  $y$ -direction. In addition, a contribution to the reconstructed  $\omega = 0$  peak is given by events having tiny  $\omega$  values, as proved by the deficit in their reconstructed angles, also visible in the plots in Fig. 8.

Further on, we investigated the variation of  $P_l A$  values on energy and polarization. Figure 9 presents the obtained  $P_l A$  results, for the entire energy range

and four polarization values: 0.25, 0.5, 0.75 and 1, in addition to  $P_l A = 0$  needed by the reconstruction of the offset values. Regarding the propagation of B-related uncertainties in the polarization measurement, we considered conservatively a total correlation between  $B$  uncertainties and  $A$  uncertainties. We took this approach since, although according to the model defined as Eq. (4) the analyzing power  $A$  and the offset value  $B$  are parameterized as independent coefficients of different order as a function of gamma-ray polarization  $P_l$ , they are not necessarily independent as functions of the azimuthal angle. Even in such a conservative error evaluation, the GPE is capable of probing several interesting phenomena at 3 sigma statistical significance, as detailed in the next section.

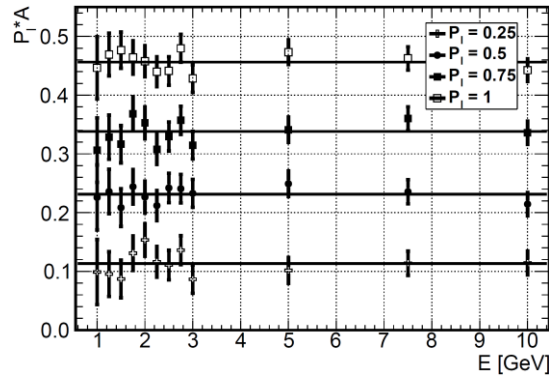


Fig. 9 –The variation of  $P_l A$  parameter obtained from fits on azimuthal angle distributions for the four non-zero polarization values: 0.25 (empty crosses), 0.5 (filled circles), 0.75 (filled squares) and 1 (empty squares) function of  $E$ , for the considered energy range: 1–10 GeV. Each set of values is averaged and a line is plotted. The value for  $P_l = 0$  ( $B$ ) is subtracted from the  $P_l A$  values for these non-zero polarizations.

As it can be inferred from the plot in Fig. 9,  $P_l A$  values are independent of gamma-ray energy within the error bars, which means that the analyzing power is independent of the energy.

#### 4. CAPABILITY FOR EXPERIMENTS WITH LASERS AT ELI-NP

##### 4.1. RADIATION REACTION

The simultaneous measurement of both energy and polarization of GeV gammas is required by radiation-reaction investigations [22, 23] and the study of the pair-production emission in strong laser fields [22]. In the case of the radiation-reaction, the effect is based on the interaction between an intense laser field and an accelerated electron beam, and it has as signature a strong gamma emission. The

electron beam can be provided by a conventional accelerator or by an additional laser, *via* the LWFA process [3, 23].

Several theoretical models have been proposed [23] for the description of this effect – for example a simulation done at ELI-NP [23] predicts a dramatic decrease in the electron energy and the dependence of the gamma photon polarization on its energy, as a consequence of the radiation reaction. In the case of 5 GeV electrons and  $10^{22}$  W/cm<sup>2</sup> laser intensity, the gamma polarization varies from 0.8 to less than 0.1 for decreasing energy, and a decrease in the electron energy of more than 80% is foreseen. Applying a simple Z-test analysis on these predictions, a GPE polarization measurement using  $10^4$  reconstructed events, could provide a better than 5 sigma significance for the detection of the radiation reaction effect (Z-test value =  $-9.22$ ) assuming that  $P_l A = 0.390 \pm 0.027$  decreases to  $P_l A = 0.071 \pm 0.022$ .

#### 4.2. THE BIREFRINGENCE OF THE QED VACUUM

Exposed to a strong electromagnetic field, the vacuum properties suffer modifications, as described by the QED theory [25, 26]. Even at  $\sim 10^{22} - 10^{23}$  W/cm<sup>2</sup> laser intensity, achievable at ELI-NP, a polarization-dependent modification of refractive index of the vacuum is predicted, and can be probed by the combination between a laser field and a linearly polarized gamma beam, having energy in the GeV range [8, 27].

This effect, known as “vacuum birefringence”, can be demonstrated by a change in the gamma polarization state after passing through the tight focus region with ultra-high laser intensity, a parameter measurable by the GPE detector. A detailed description on the vacuum birefringence has been provided in [8], and the conceptual design of a detector able to provide this measurement at ELI-NP was developed in [28, 29].

The estimation presented in [8] predicts a variation in the gamma-ray polarization from 0.97 to 0.53 for 1 GeV gammas, when the vacuum polarization effect is present. Applying the simulations presented in Section 3 to  $8 \times 10^3$  reconstructed events, the azimuthal angle parameters increase from  $P_l A = 0.211 \pm 0.043$  for  $P_l = 0.53$  to  $P_l A = 0.416 \pm 0.042$  for  $P_l = 0.97$ , resulting a Z-test value of  $-3.37$  and a better than 3 sigma significance for the measurement of this effect.

#### 4.3. OTHER EXPERIMENTS AT ELI-NP

In addition to these two applications, GPE could be used in experiments aiming to detect the muon production in laser interactions [30, 31] and in experiments focused on the GeV gamma generation at very high laser intensities, of the order of  $10^{23}$  W/cm<sup>2</sup> [32], in the interaction with solid targets.

Several such experiments are proposed at ELI-NP, and detailed feasibility studies are ongoing for these measurements, which will have to overcome key

background-related issues, such as reconstructing a low number of muon events out of a significant background of high energy electrons, in the case of muon generation.

## 5. CONCLUSIONS

Although polarimeters for high energy gamma rays are nowadays developed mainly for astrophysical searches, further applications to the investigation of laser-matter interaction are described in this paper, in the framework of the developments of new, unique experimental capabilities at the ELI-NP facility.

The capabilities of a compact gamma-ray detector able to measure both the polarization and energy of gamma photons is shown in the range of 1 to 10 GeV, relevant for several experiments envisaged to take place at high-power laser facilities. The detector has been assembled at ELI-NP and has been tested with cosmogenic muons. The performances for gamma polarimetry and energy measurements, as reported in this work, have been evaluated from extensive Geant4 simulations, the energy resolution being found to be better than 15% and the analyzing power approximately 0.5. These performances were discussed in comparison with the requirements for some of the scientific subjects foreseen at ELI-NP. In-beam tests of the detector will take place at a gamma beam facility (such as SPring8/LEPS) in the near future.

Further potential developments of the GPE are studied together with our collaborators from KEK and Hiroshima University, Japan, targeting the increase of the applicable range of energies and of the gamma fluxes able to be accommodated.

*Acknowledgements.* The authors wish to thank to Dr. Madalin Rosu, Dr. Keita Seto and Mr. Jonathan Tamlyn from ELI-NP for fruitful discussions and their support in the construction of the detector. This work was carried out with the support of contract PN 23 21 01 05 funded by the Romanian Ministry of Research, Innovation and Digitalization and by the Extreme Light Infrastructure Nuclear Physics Phase II, a project co-financed by the Romanian Government and the European Union through the European Regional Development Fund and the Competitiveness Operational Programme (No. 1/07.07.2016, COP, ID 1334).

## REFERENCES

1. K. Tanaka *et al.*, Matter and Radiation at Extremes **5**, 024402 (2020).
2. J. Schwinger, Phys. Rev. **82**, 664 (1951).
3. T. Tajima and J. M. Dawson, Physical Review Letters, **43**(4), 267–270 (1979).
4. C.N. Yang, Phys. Rev. **77**, 722 (1950).
5. T.H. Berlin, L. Madansky, Phys. Rev. **78**, 623 (1950).
6. L.C. Maximon and H. Olsen, Phys. Rev. **126**, 310 (1962).
7. P. Gros and D. Bernard, Astroparticle Physics **88**, 30–37 (2017).
8. Y. Nakamiya and K. Homma, Phys. Rev. D **96**, 053002 (2017).
9. C. Ilie, PASP **131**, 111001 (2019).
10. P. Gros, S. Amano, D. Attié *et al.*, Astroparticle Physics **97**, 10–18 (2018).

11. C. d. Jager *et al.*, *Eur. Phys. J. A* **19**, 1 (2004).
12. M. Cuciuc *et al.*, “Gamma Polari-Calorimeter, an instrument for gamma ray polarimetry using the pair production process”, talk at Light driven Nuclear-Particle Physics and Cosmology 2017 (LNPC’17), April 19th-21st, 2017.
13. Y. Arai, INTPIX4 User’s Manual, <http://rd.kek.jp/project/soi/> Revision 0.33 (2013).
14. R. Nishimura, Y. Arai, T. Miyoshi, K. Hirano, S. Kishimoto, and R. Hashimoto, *Nuclear Instruments and Methods in Physics Research A* **831**, 49–54 (2016).
15. <https://research.kek.jp/people/tauchik/seabas2/>
16. T. Uchida, *IEEE Trans. Nucl. Sci.* **55** (3), 1631–1637 (2008).
17. Detector Technology Project International Review Committee 2013, December 10–11, 2013, Part I, SOI, document available at: [https://rd.kek.jp/project/soi/documents/1312\\_DTP\\_Report\\_SOI.pdf](https://rd.kek.jp/project/soi/documents/1312_DTP_Report_SOI.pdf)
18. R. Brun and F. Rademakers, “ROOT – An Object Oriented Data Analysis Framework”, Proceedings AIHENP’96 Workshop, Lausanne, Sep. 1996, *Nucl. Inst. & Meth. in Phys. Res. A* **389** 81–86 (1997). See also <https://root.cern/>
19. S. Agostinelli *et al.*, *Nuclear Instruments and Methods in Physics Research A* **506**, 250–303 (2003).
20. J. Allison *et al.*, *IEEE Transactions on Nuclear Science* **53**, 270–278 (2006).
21. J. Allison *et al.*, *Nuclear Instruments and Methods in Physics Research A* **835**, 186–225 (2016).
22. K. Homma *et al.*, *Romanian Reports in Physics* **68**, S233–S274 (2016).
23. K. Seto *et al.*, *High Energy Density Physics* **38**, 100919 (2021).
24. K. Homma, K. Seto, and O. Tesileanu, “Combined Laser Gamma Experiments at ELI-NP”, ELI-NP internal document, 2015.
25. W. Dittrich and H. Gies, *Probing the Quantum Vacuum*, Springer, Berlin, Heidelberg, 2000.
26. J. Schwinger, *Phys. Rev.* **82**, 664 (1951).
27. K. Homma, D. Habs, T. Tajima, *Appl. Phys. B* **104**, 769–782 (2011).
28. K. Homma and Y. Nakamiya, “Gamma Polari-Calorimetry with SOI pixels for proposals at Extreme Light Infrastructure (ELI-NP)”, International Workshop on SOI Pixel Detector (2015).
29. M. Cuciuc *et al.*, *IEEE Nuclear Science Symposium and Medical Imaging Conference (NSS/MIC)*, 2017, pp. 1–3, DOI: 10.1109/NSSMIC.2017.8532591.
30. A. Titov *et al.*, *Phys. Rev. Spec. Top.* **12**, 111301 (2009).
31. B.S. Rao *et al.*, “Bright muon source driven by GeV electron beams from a compact laser wakefield accelerator”, arXiv:1804.03886 [physics.plasm-ph].
32. T. Nakamura, J. K. Koga, T. Z. Esirkepov, M. Kando, G. Korn, and S. V. Bulanov, *Phys. Rev. Lett.* **108**, 195001 (2012).